

# Altitude effects of localized source currents on magnetotelluric responses

Shinya Sato

Graduate School of Engineering, Kyoto University

Email: [sato.shinya.27s@st.kyoto-u.ac.jp](mailto:sato.shinya.27s@st.kyoto-u.ac.jp)

## Abstract

The effects of localized source currents on Earth's magnetotelluric (MT) responses have been evaluated in terms of the changes in period and subsurface structure. The focus is on the bias within the MT responses arising from variations in the vertical and horizontal distances of the source current. The MT responses at 20 and 200 s are calculated at various distances from the source current. A slight change in the source's distance causes a shift in the MT responses, and the bias is large, especially over the altitude explored in the MT data analysis (i.e., 100–150 km), where the E layer exists. The vertical distance of the source field varies because the distribution of conductivity with altitude in the ionosphere and the region controlling the ionospheric electrical process change temporally. Thus, in assessing the temporal changes in MT responses, we should treat them carefully with checking ionospheric environment.

## Introduction

In magnetotelluric (MT) surveys, the primary source magnetic fields are assumed horizontally uniform. The effects of localized source currents on the MT responses have been discussed in the literature (Madden and Nelson, 1964; Schmucker, 1970; Hermance and Peltier, 1970; Häkkinen et al., 1989; Pirjola, 1992; Viljanen, 2012), where impedances over long periods and at sites above structures of high resistivity are biased because of the collapse of the plane-wave assumption. For example, Pirjola (1992) calculated the downward/upward bias of the apparent resistivities in the range of 1–100,000 s due to the electrojet with field-aligned currents under the condition that the divergence of the total current density vanishes. The study reported that the apparent resistivity of 100  $\Omega\text{m}$  and at periods larger than 60 s were clearly affected. Although past studies focused on period-dependent bias, the bias stemming from the variation in distances, especially altitudes, of the localized source currents was not discussed in detail.

Temporal/seasonal changes (Brändlein et al., 2012; Romano et al., 2014; Vargas and Ritter, 2016) and bias (Murphy and Egbert, 2018) in the MT responses/vertical geomagnetic transfer-functions due to the source field have been recently reported. For example, Romano et al. (2014) reported that, for time periods 20–100 s, the apparent resistivities have a negative correlation with geomagnetic activity. In particular, in time-lapse MT sounding, the source bias on the MT responses

is critical because we suppose the temporal changes in impedances due to the source field to be changes in subsurface resistivity.

In this study, the electromagnetic fields and MT responses were calculated by varying the vertical and horizontal distances of the source current. The study revealed: i) the numerical examples of the bias in the MT responses because of the variation in vertical and horizontal distances of the source field, ii) implications from these examples, iii) the mathematical underpinning of this bias, and iv) the mathematical conditions for upholding the plane-wave assumption.

### Electromagnetic fields above Earth's surface

We chose a Cartesian coordinate system, where the  $x$ ,  $y$ , and  $z$  axes are northward, westward, and downward positive, respectively, with  $z = 0$  at Earth's surface. The coordinate system, the line source current to be defined later, and an observation site are depicted in Fig. 1.

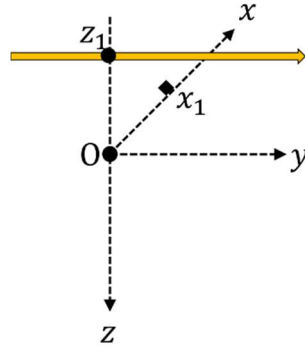


Figure 1. Coordinate system used in this study. The symbol of “O” and diamond symbols mark the origin and an observation site, respectively;  $z_1$  and  $x_1$  are the altitude of the line current and the horizontal distance of an observed site, respectively.

Ignoring the displacement current and using the SI system, Maxwell's equations in the frequency domain are

$$\nabla \times \mathbf{E} = -i\omega\mathbf{B}, \quad (1)$$

$$\nabla \times \mathbf{B} = \mu_0(\sigma\mathbf{E} + \mathbf{J}), \quad (2)$$

$$\nabla \cdot \mathbf{B} = 0, \quad (3)$$

where  $\mathbf{E}$ ,  $\mathbf{B}$ , and  $\mathbf{J}$  are the electric field, magnetic induction, and source current, respectively;  $\sigma$ ,  $\mu_0$ , and  $\omega$  are the electrical conductivity, the magnetic permeability of free space, and the angular frequency, respectively. Introducing the vector potential  $\mathbf{A}$  and the scalar potential  $\Pi$ , the electromagnetic fields are

$$\mathbf{B} = \nabla \times \mathbf{A}, \quad (4)$$

$$\mathbf{E} = -i\omega(\mathbf{A} + \nabla\Pi). \quad (5)$$

We apply a gauge transformation such that  $\mathbf{A}$  and  $\Pi$  satisfy

$$i\omega\sigma\mu_0\Pi = -\nabla \cdot \mathbf{A}, \quad (6)$$

and the equation for the vector potential can be represented as

$$-\Delta\mathbf{A} + i\omega\sigma\mu_0\mathbf{A} = \mu_0\mathbf{J}. \quad (7)$$

Because  $\nabla \cdot \mathbf{E} = 0$ , the equation for the scalar potential,

$$-\Delta\Pi + i\omega\sigma\mu_0\Pi = 0, \quad (8)$$

holds. Considering the electromagnetic fields above Earth's surface (i.e.,  $z \leq 0$ ),  $\sigma$  may be taken as  $\sigma_0$  denoting the electrical conductivity of free space.

As in the analysis in Hermance and Peltier (1970), we consider a wire at an altitude  $z_1 < 0$  carrying an electric current  $I$  (Fig. 1); the current density is

$$\mathbf{J} = \begin{pmatrix} J_x \\ J_y \\ J_z \end{pmatrix} = I\delta(z - z_1)\delta(x) \begin{pmatrix} 0 \\ 1 \\ 0 \end{pmatrix}. \quad (9)$$

We focus on only  $A_y$ , the  $y$  component of  $\mathbf{A}$ , and  $\Pi$ . For this study, the application of the Fourier transform (FT) to the horizontal components transforms  $x$  and  $y$  into the wavenumber domain yielding

$$\tilde{F}(\eta, \zeta) = \int_{-\infty}^{\infty} \int_{-\infty}^{\infty} F(x, y) e^{i(\eta x + \zeta y)} dx dy, \quad (10)$$

$$F(x, y) = \frac{1}{4\pi^2} \int_{-\infty}^{\infty} \int_{-\infty}^{\infty} \tilde{F}(\eta, \zeta) e^{-i(\eta x + \zeta y)} d\eta d\zeta. \quad (11)$$

Eq. 11 enables us to transform Eq. 7 into

$$\frac{\partial}{\partial z^2} \tilde{A}_y - \beta_0^2 \tilde{A}_y = -\mu_0 \tilde{J}_y \quad (z \leq 0), \quad (12)$$

where  $\tilde{A}_y$  and  $\tilde{J}_y$  are  $A_y$  and  $J_y$  in the wavenumber domain, respectively, and  $\beta_0 = \sqrt{(\eta^2 + \zeta^2) + i\omega\mu_0\sigma_0}$ . Eq. 12 is the Helmholtz equation and for which its Green's function satisfies

$$\frac{\partial}{\partial z^2} G(z, z') - \beta_0^2 G(z, z') = \delta(z - z'). \quad (13)$$

As shown in Arfken et al. (2012), the solution of  $G(z, z')$  is

$$G(z, z') = -\frac{(e^{-\beta_0|z-z'|} + \Lambda e^{-\beta_0|z+z'|})}{2\beta_0}, \quad (14)$$

where  $\Lambda$  is a constant required to uphold the boundary condition at  $z = 0$ . Consider a structure beneath Earth's surface ( $z > 0$ ) having a half-space of conductivity  $\sigma_1$ . The continuity of the electromagnetic fields parallel to the boundary yields

$$\Lambda(\eta, \zeta) = \frac{\beta_0 - \beta_1}{\beta_0 + \beta_1}, \quad (15)$$

where  $\beta_1 = \sqrt{(\eta^2 + \zeta^2) + i\omega\mu_0\sigma_1}$ . Applying the FT to the horizontal components, Eq. 10,  $\tilde{J}_y$  in Eq. 12 becomes

$$\tilde{J}_y = 2\pi I \delta(z - z_1) \delta(\zeta). \quad (16)$$

Using Green's function, the solutions for  $\tilde{A}_y$  are

$$\tilde{A}_y = \pi\mu_0 I \frac{(e^{-\beta_0|z-z_1|} + \Lambda e^{-\beta_0|z+z_1|})\delta(\zeta)}{\beta_0}. \quad (17)$$

Similarly, applying the inverse FT to the horizontal components, Eq. 11, and considering  $\sigma_0 = 0$ ,  $A_y$  is written as

$$A_y = \frac{\mu_0 I}{4\pi} \int_{-\infty}^{\infty} \frac{(e^{-|\eta|(z-z_1)} + \Lambda(\eta, 0)e^{|\eta|(z+z_1)})}{|\eta|} e^{-i\eta x} d\eta \quad (z \leq 0). \quad (18)$$

The vector potential  $\mathbf{A}$  has only a  $y$ -component and  $A_y$  is independent of  $y$ . As a result, the divergence of  $\mathbf{A}$  is equal to zero, and the scalar potential is ignored because both sides of Eq. 6 vanish. From Eqs. 4 and 5, the magnetic induction  $B_x$  and the electric field  $E_y$  of a site ( $x = x_1$ ) at Earth's surface ( $z = 0$ ) is written as

$$B_x = \frac{\mu_0 I}{2\pi} \int_{-\infty}^{\infty} \frac{\sqrt{\eta^2 + i\omega\mu_0\sigma_1}}{|\eta| + \sqrt{\eta^2 + i\omega\mu_0\sigma_1}} e^{|\eta|z_1} e^{-i\eta x_1} d\eta, \quad (19)$$

$$E_y = -i\omega \frac{\mu_0 I}{2\pi} \int_{-\infty}^{\infty} \frac{1}{|\eta| + \sqrt{\eta^2 + i\omega\mu_0\sigma_1}} e^{|\eta|z_1} e^{-i\eta x_1} d\eta. \quad (20)$$

Taking their ratio  $E_y/B_x$  gives the impedance  $Z_{yx}$

$$Z_{yx} = \frac{-i\omega \int_{-\infty}^{\infty} \frac{1}{|\eta| + \sqrt{\eta^2 + i\omega\mu_0\sigma_1}} e^{|\eta|z_1} e^{-i\eta x_1} d\eta}{\int_{-\infty}^{\infty} \frac{\sqrt{\eta^2 + i\omega\mu_0\sigma_1}}{|\eta| + \sqrt{\eta^2 + i\omega\mu_0\sigma_1}} e^{|\eta|z_1} e^{-i\eta x_1} d\eta}. \quad (21)$$

For this study, the apparent resistivity  $\rho_{yx}$  is given by

$$\rho_{yx} = \frac{\mu_0}{2\pi f} |Z_{yx}|^2, \quad (22)$$

where  $Z_{yx}$  is defined in Eq. 21. Note that hereafter, for simplicity,  $x_1$  is defined as the horizontal distance to the source current; the distance unit used is "km" instead of "m" when stating horizontal/vertical distances ( $x_1, z_1$ ) although all the above values are calculated using the SI system of units.

### MT responses biased by source line current

Here, the subsurface resistivity and the time period are set to 1000  $\Omega\text{m}$  (i.e.,  $\sigma_1 = 10^{-3}$  S/m) and 20 s, respectively. The subsurface resistivity has the same value as that used for the crust in Hermance and Peltier (1970).

By changing the altitude of the source current  $z_1$  from  $-100$  to  $-1000$  km in increments of 5 km and the horizontal distances  $x_1 = 1, 5, 10, 50, 100, 500, 1000,$  and  $5000$  km, the variation in the field components  $B_x$  (Eq. 19) and  $E_y$  (Eq. 20) as well as the impedance  $Z_{yx}$  (Eq. 21) were determined. The integrals in Eqs. 19 and 20 were calculated using the discrete approximation; the convergence of each was verified. Note that the electric current  $I$  in Eq. 9 is 1000 A although the

value has no influence on  $Z_{yx}$ . The calculated values of the apparent resistivity (Eq. 22) and phase are shown in Fig. 2.

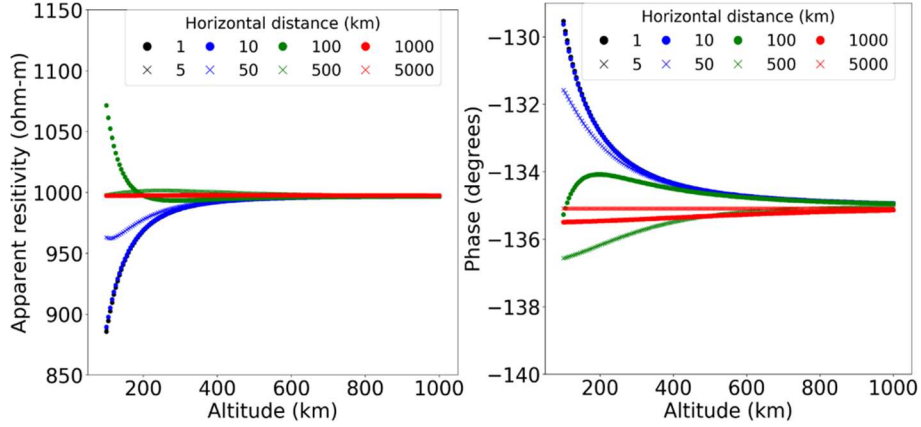


Figure 2. MT responses for a time period of 20 s: (left) Relationship between the apparent resistivity and the altitude of the source current. (right) Relationship between the phase and the altitude of source current. The black/blue/green/red circles denote the responses derived from the horizontal distances of 1/10/100/1000 km, respectively. The black/blue/green/red crosses denote the responses derived from the horizontal distances of 5/50/500/5000 km, respectively.

In addition, the values of the apparent resistivity and phase are derived by varying  $x_1$  from 0 to 3000 km in increments of 10 km and  $z_1$  set to  $z_1 = -100, -150, -200, -500,$  and  $-1000$  km (Fig. 3).

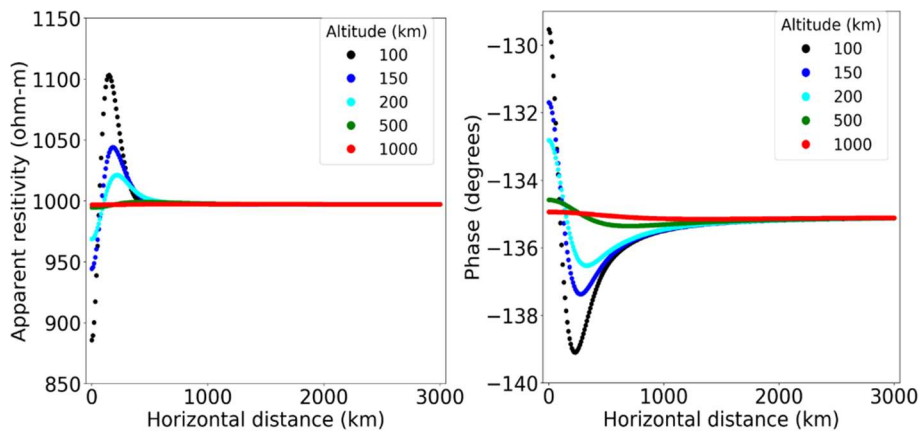


Figure 3. MT responses for a time period of 20 s: (left) Relationship between the apparent resistivity and the horizontal distance of source current. (right) Relationship between the phase and the horizontal distance of source current. The black/blue/light blue/green/red circles denote the responses derived from the altitude of 100/150/200/500/1000 km, respectively.

On the basis of these results (Figs. 2 and 3), the MT responses are shifted largely depending on the

vertical and horizontal distances from the source current, if the altitude is within the range 100–150 km where the E region (Viljanen, 2012; Sheng et al., 2014) with an important current system for MT exists. However, if  $x_1$  and  $|z_1|$  are larger, such bias becomes smaller.

The MT responses at a time period of 200 s under the same conditions as the above were plotted (Figs. 4 and 5) and, as expected, are biased by the source current more than those of Figs. 2 and 3.

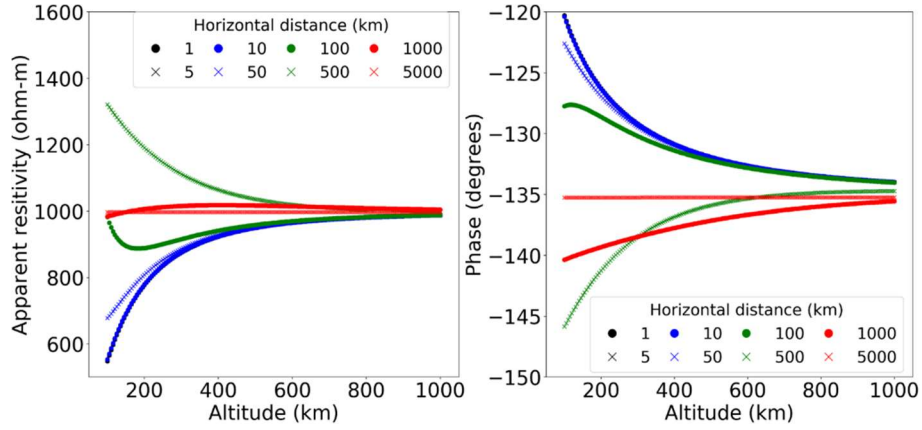


Figure 4. As for Fig. 2 except the MT responses for a time period of 200 s.

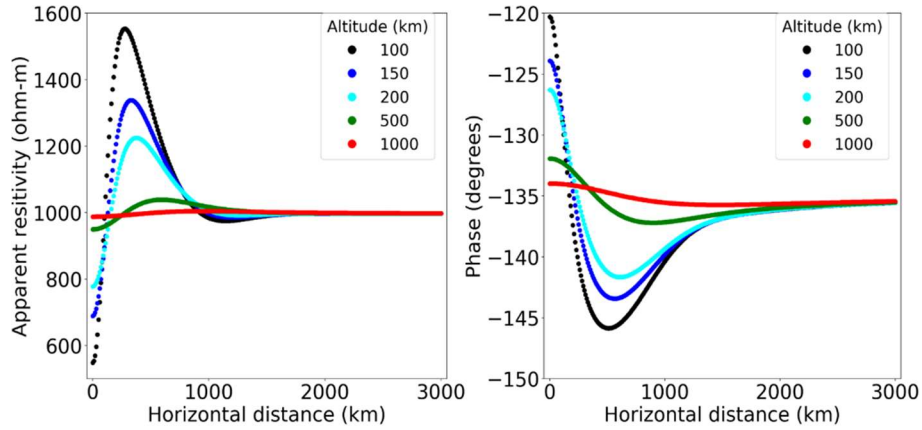


Figure 5. As for Fig. 3 except the MT responses for a time period of 200 s.

## Discussion

A discussion is presented next of i) the mathematical basis of the bias on the MT responses due to the source field, ii) the mathematical condition upholding the plane-wave assumption, and iii) the implication arising from the numerical examples performed in this study.

The electromagnetic fields (Eqs. 19 and 20) generated by the line source current have an attenuation term

$$\alpha(\eta) = e^{|\eta|z_1}, \quad (23)$$

and a term conveying information regarding the subsurface structure

$$\beta(\eta) = \sqrt{\eta^2 + i\omega\mu_0\sigma_1}. \quad (24)$$

Substituting  $\frac{2\pi}{20}$  1/s,  $1.26 \cdot 10^{-6}$  H/m, and 0.001 S/m for  $\omega$ ,  $\mu_0$ , and  $\sigma_1$ , respectively, the apparent resistivity and phase were plotted (Figs. 2 and 3). When the wavenumber  $|\eta|$  is greater than  $2.0 \cdot 10^{-5}$ , the influence of  $\eta$  is greater than  $\omega\mu_0\sigma_1$ . If  $|\eta|$  vanishes,  $\alpha(\eta) = 1$  and the wavenumber effect on  $\beta(\eta)$  vanishes. Hence, we set  $\alpha(\eta) = 1$  for the standard. When  $\alpha(\eta)$  in Eq. 23 is smaller than 0.01, the effect of  $|\eta|$  is assumed negligible because the attenuation term  $\alpha(\eta)$  is two orders of magnitude smaller than the standard (i.e.,  $\alpha(\eta) = 1$ ). To uphold this assumption,  $|\eta|z_1$  should be smaller than  $-4.6$ , and when  $z_1 = -100$  km,  $|\eta|$  should be greater than  $4.6 \cdot 10^{-5}$ . Therefore, the integrands in Eqs. 19 and 20 are biased by wavenumber  $|\eta|$  at least within the interval  $2.0 \cdot 10^{-5} < |\eta| < 4.6 \cdot 10^{-5}$ . However, given that  $z_1 = -1000$  km,  $\alpha(\eta) \leq 2.1 \cdot 10^{-9}$  when substituting  $|\eta| \geq 2.0 \cdot 10^{-5}$ , which yields a greater effect than  $\omega\mu_0\sigma_1$ . The wavenumber effect is small enough to be negligible, and as a result, the apparent resistivity approaches a constant value of 1000  $\Omega\text{m}$ , i.e., the subsurface resistivity. As expected from the above discussion, the MT responses at 200 s are biased more than those at 20 s because the influence of  $\eta$  is greater than  $\omega\mu_0\sigma_1$  when  $|\eta|$  is greater than  $6.3 \cdot 10^{-6}$ .

Both responses at 20 and 200 s indicate the same patterns of bias; that is, they shift depending not only on the vertical ( $z_1$ ) but also on the horizontal distance ( $x_1$ ) between the site and the source current. The integrands in Eqs. 19 and 20 oscillate because of the factor  $e^{-i\eta x_1}$ , and substituting 5000 km into  $x_1$ , the apparent resistivity (Eq. 22) at 20/200 s have values of 1000  $\Omega\text{m}$  (see Figs. 2 and 4). The mathematics behind these calculated results resides with the re-expressions of Eqs. 19 and 20

$$B_x = \frac{\mu_0 I}{\pi} \int_0^\infty \frac{\sqrt{\eta^2 + ia}}{\eta + \sqrt{\eta^2 + ia}} (e^{\eta(z_1 - ix_1)} + e^{\eta(z_1 + ix_1)}) d\eta, \quad (25)$$

$$E_y = -i\omega \frac{\mu_0 I}{\pi} \int_0^\infty \frac{1}{\eta + \sqrt{\eta^2 + ia}} (e^{\eta(z_1 - ix_1)} + e^{\eta(z_1 + ix_1)}) d\eta, \quad (26)$$

where  $a = \omega\mu_0\sigma_1$ . Focusing on the term with  $e^{\eta(z_1 - ix_1)}$  and integrating by parts, we can obtain,

$$\int_0^\infty \frac{\sqrt{\eta^2 + ia}}{\eta + \sqrt{\eta^2 + ia}} e^{\eta(z_1 - ix_1)} d\eta \quad (27)$$

$$= \frac{-1}{(z_1 + ix_1)} + \frac{-1}{\sqrt{ia}(z_1 + ix_1)^2} + \frac{-2}{ia(z_1 + ix_1)^3} - \int_0^\infty \frac{d^3}{d\eta^3} \left( \frac{\sqrt{\eta^2 + ia}}{\eta + \sqrt{\eta^2 + ia}} \right) \frac{e^{\eta(z_1 - ix_1)}}{(z_1 - ix_1)^3} d\eta,$$

$$\int_0^\infty \frac{e^{\eta(z_1 - ix_1)}}{\eta + \sqrt{\eta^2 + ia}} d\eta \quad (28)$$

$$= \frac{-1}{\sqrt{ia}(z_1 + ix_1)} + \frac{-1}{ia(z_1 + ix_1)^2} + \frac{-1}{(ia)^{\frac{3}{2}}(z_1 + ix_1)^3} - \int_0^\infty \frac{d^3}{d\eta^3} \left( \frac{1}{\eta + \sqrt{\eta^2 + ia}} \right) \frac{e^{\eta(z_1 - ix_1)}}{(z_1 - ix_1)^3} d\eta.$$

The triangle inequality and the inequality  $\left| \frac{1}{(\eta^2 + ia)} \right| \leq \frac{1}{a}$  ( $\eta \in \mathbb{R}$ ) enable the integrands of the last

terms in Eqs. 27 and 28 to be examined

$$\left| \frac{d^3}{d\eta^3} \left( \frac{\sqrt{\eta^2+ia}}{\eta+\sqrt{\eta^2+ia}} \right) \right| = \left| \frac{3(\eta-\sqrt{\eta^2+ia})}{(\eta+\sqrt{\eta^2+ia})(\eta^2+ia)^{\frac{3}{2}}} \left\{ 1 + \frac{\eta(\eta+2\sqrt{\eta^2+ia})}{(\eta^2+ia)} \right\} \right| \quad (29)$$

$$\left| \frac{d^3}{d\eta^3} \left( \frac{\sqrt{\eta^2+ia}}{\eta+\sqrt{\eta^2+ia}} \right) \right| \leq \frac{6\eta+3a}{a^2} \left( 1 + \frac{3\eta^2+2\sqrt{a}\eta}{a} \right),$$

$$\left| \frac{d^3}{d\eta^3} \left( \frac{1}{\eta+\sqrt{\eta^2+ia}} \right) \right| = \left| \frac{-3\eta}{(\eta^2+ia)^{\frac{5}{2}}} \right| \leq \frac{3\eta}{a^2}. \quad (30)$$

Eqs. 29 and 30 and the inequality  $|\int_0^\infty F(\eta)d\eta| \leq \int_0^\infty |F(\eta)|d\eta$ , where  $F$  is an arbitrary function, give

$$\left| \int_0^\infty \frac{d^3}{d\eta^3} \left( \frac{\sqrt{\eta^2+ia}}{\eta+\sqrt{\eta^2+ia}} \right) e^{\eta(z_1-ix_1)} d\eta \right| \leq \int_0^\infty \frac{6\eta+3a}{a^2} \left( 1 + \frac{3\eta^2+2\sqrt{a}\eta}{a} \right) e^{\eta z_1} d\eta, \quad (31)$$

$$\left| \int_0^\infty \frac{d^3}{d\eta^3} \left( \frac{1}{\eta+\sqrt{\eta^2+ia}} \right) e^{\eta(z_1-ix_1)} d\eta \right| \leq \int_0^\infty \frac{3\eta}{a^2} e^{\eta z_1} d\eta. \quad (32)$$

The right-hand sides of Eqs. 31 and 32 are constant and do not diverge. Replacing

$$\int_0^\infty \frac{d^3}{d\eta^3} \left( \frac{\sqrt{\eta^2+ia}}{\eta+\sqrt{\eta^2+ia}} \right) e^{\eta(z_1-ix_1)} d\eta \quad \text{and} \quad \int_0^\infty \frac{d^3}{d\eta^3} \left( \frac{1}{\eta+\sqrt{\eta^2+ia}} \right) e^{\eta(z_1-ix_1)} d\eta$$

with  $C_1$  and  $D_1$ , respectively, the absolute values  $|C_1|$  and  $|D_1|$  are always less than a constant value. The same applies to

$$\int_0^\infty \frac{\sqrt{\eta^2+ia}}{\eta+\sqrt{\eta^2+ia}} e^{\eta(z_1+ix_1)} d\eta \quad \text{and} \quad \int_0^\infty \frac{e^{\eta(z_1+ix_1)}}{\eta+\sqrt{\eta^2+ia}} d\eta, \quad \text{with} \quad \int_0^\infty \frac{d^3}{d\eta^3} \left( \frac{\sqrt{\eta^2+ia}}{\eta+\sqrt{\eta^2+ia}} \right) e^{\eta(z_1-ix_1)} d\eta$$

$$\int_0^\infty \frac{d^3}{d\eta^3} \left( \frac{1}{\eta+\sqrt{\eta^2+ia}} \right) e^{\eta(z_1-ix_1)} d\eta$$

being replaced by  $C_2$  and  $D_2$ , respectively. As a result, the electromagnetic fields take the form

$$B_x = -\frac{\mu_0 I}{\pi} \left\{ \frac{1}{(z_1+ix_1)} + \frac{1}{\sqrt{ia}(z_1+ix_1)^2} + \frac{2+iaC_1}{ia(z_1+ix_1)^3} + \frac{1}{(z_1-ix_1)} + \frac{1}{\sqrt{ia}(z_1-ix_1)^2} + \frac{2+iaC_2}{ia(z_1-ix_1)^3} \right\}, \quad (33)$$

$$E_y = i\omega \frac{\mu_0 I}{\pi} \left\{ \frac{1}{\sqrt{ia}(z_1+ix_1)} + \frac{1}{ia(z_1+ix_1)^2} + \frac{1+(ia)^{\frac{3}{2}}D_1}{(ia)^{\frac{3}{2}}(z_1+ix_1)^3} + \frac{1}{\sqrt{ia}(z_1-ix_1)} + \frac{1}{ia(z_1-ix_1)^2} + \right. \quad (34)$$

$$\left. \frac{1+(ia)^{\frac{3}{2}}D_2}{(ia)^{\frac{3}{2}}(z_1-ix_1)^3} \right\}.$$

Using Eqs. 33 and 34,  $Z_{yx}$  in Eq. 21 is written as

$$Z_{yx} = -i\omega \frac{\left\{ \frac{1}{\sqrt{ia}(z_1+ix_1)} + \frac{1}{ia(z_1+ix_1)^2} + \frac{1+(ia)^{\frac{3}{2}}D_1}{(ia)^{\frac{3}{2}}(z_1+ix_1)^3} + \frac{1}{\sqrt{ia}(z_1-ix_1)} + \frac{1}{ia(z_1-ix_1)^2} + \frac{1+(ia)^{\frac{3}{2}}D_2}{(ia)^{\frac{3}{2}}(z_1-ix_1)^3} \right\}}{\left\{ \frac{1}{(z_1+ix_1)} + \frac{1}{\sqrt{ia}(z_1+ix_1)^2} + \frac{2+iaC_1}{ia(z_1+ix_1)^3} + \frac{1}{(z_1-ix_1)} + \frac{1}{\sqrt{ia}(z_1-ix_1)^2} + \frac{2+iaC_2}{ia(z_1-ix_1)^3} \right\}}. \quad (35)$$

In the limit  $x_1 \rightarrow \infty$ , the plane-wave assumption is established

$$Z_{yx} = -\frac{i\omega}{\sqrt{ia}} = \frac{-\sqrt{i\omega}}{\sqrt{\mu_0\sigma_1}}, \quad (36)$$

which is also upheld in the limit  $z_1 \rightarrow -\infty$ . This means that if either the horizontal or vertical distance

of the localized current is large enough, the plane-wave assumption remains valid. If this condition is not established, the MT responses would be biased by the source field (see Figs. 2–5).

In this study, the focus was on the relationship between the MT responses and the vertical/horizontal of the source current. On the basis of the numerical simulations (Figs. 2–5) and the above discussions, the source bias becomes smaller if the altitude of line source current is higher, but becomes large especially when the altitude is within 100–150 km. The altitude distribution of the conductivity in the ionosphere changes temporally/seasonally (Sheng et al., 2014). As shown in Du and Stening (1999), the E and F layers control the ionospheric electrical process during daytime and nighttime, respectively. Therefore, the altitude of the source current may be considered to vary temporally. Considering that the E and F layers are at the altitudes of 100–150 km and 150–600 km (Sheng et al., 2014), respectively, the MT data measured during nighttime possibly weaken the source bias if we use only the line current in the ionosphere for a source. Additionally, if deriving MT responses using many spectra (i.e., long time-series data), this source bias may be neglected because the electromagnetic fields generated by the localized current are averaged. However, in the estimation of MT impedances from short-term data, the source effect must be considered because the electrical environment in the ionosphere mentioned above changes with a period of several hours to several months. For time-lapse MT especially, the bias should be considered as reported by Romano et al. (2014). Moreover, considering that the range in biased apparent resistivities at 200 s is 550–1,550  $\Omega\text{m}$  (Fig. 5), the MT responses from short-term data should be used carefully for the inversion.

The line source current defined by Eq. 9 is possibly non-realistic, and the sheet current is maybe more suitable for the actual current system. However, as reported by McNish (1938), a broad sheet-source current at higher altitude than 100 km can be approximated by a line source current. Thus, the entire discussion above derived from the assumption of line source current may be reasonable because the altitude of the line current in this study is equal to or higher than 100 km.

## Summary

In this study, the focus was on the bias in the MT responses arising from the variation in altitude and horizontal distances of a localized source current. The numerical examples show that slight changes in the distance cause a shift in the MT response especially when the altitude is within 100–150 km, where the E layer exists. These changes in MT responses are possibly seen in real MT data analysis because the vertical distance of the current source varies temporally/seasonally. Therefore, the bias in MT responses especially for time-lapse sounding should be evaluated to prevent regarding such changes arising from the source field as reflecting subsurface resistivity changes. Moreover, considering that the range in shift in MT responses, especially at long periods, depends on the distance of the source, we should treat these responses carefully for example with checking the ionospheric environment.

## **Acknowledgements**

The author thanks Dr. Tada-nori Goto, a professor at University of Hyogo, Dr. Katsuaki Koike, a professor at Kyoto University, and Mr. Fumihiko Onoue, a Ph.D. candidate at Scuola Normale Superiore di Pisa, for constructive comments.

## **Reference lists**

- Arfken GB, Weber HJ, Harris FE (2012) *Mathematical methods for physicists: A comprehensive guide*. Academic Press, Cambridge.
- Brändlein D, Lühr H, Ritter O (2012) Direct penetration of the interplanetary electric field to low geomagnetic latitudes and its effect on magnetotelluric sounding. *J Geophys Res: Space Phys* 117(A11). doi:10.1029/2012JA018008.
- Du J, Stening RJ (1999) Simulating the ionospheric dynamo—I. Simulation model and flux tube integrated conductivities. *J Atmos Sol Terr Phys* 61(12): 913-923.
- Häkkinen L, Pirjola R, Sucksdorff C (1989) EISCAT magnetometer cross and theoretical studies connected with the electrojet current system. *Geophysica* 25(1): 123-134.
- Hermance JF, Peltier WR (1970) Magnetotelluric fields of a line current. *J Geophys Res* 75(17): 3351-3356.
- Madden T, Nelson P (1964) A defense of Cagniard's magnetotelluric method. *ONR Rept*: 371-401.
- McNish AG (1938) Heights of electric currents near the Auroral Zone. *Terr. Magn. Atmos. Electr.* 43: 67-75.
- Murphy BS, Egbert GD (2018) Source biases in midlatitude magnetotelluric transfer functions due to Pc3-4 geomagnetic pulsations. *Earth Planets Space* 70(1).
- Pirjola R (1992) On magnetotelluric source effects caused by an auroral electrojet system. *Radio Sci* 27(04): 463-468.
- Romano G, Balasco M, Lapenna V, Siniscalchi A, Telesca L, Tripaldi S (2014) On the sensitivity of long-term magnetotelluric monitoring in Southern Italy and source-dependent robust single station transfer function variability. *Geophys J Int* 197(3):1425-1441.
- Schmucker U (1970) *Anomalies of geomagnetic variations in the southwestern United States*. Berkeley: Bull Scripps Inst Oceanogr.
- Sheng C, Deng Y, Yue X, Huang Y (2014) Height-integrated Pedersen conductivity in both E and F regions from COSMIC observations. *J Atmos Sol Terr Phys* 115: 79-86.
- Vargas JA, Ritter O (2016) Source effects in mid-latitude geomagnetic transfer functions. *Geophys J Int* 204(1):606-630.
- Viljanen A (2012) Description of the magnetospheric/ionospheric sources. In: Chave AD, Jones AG (ed) *The Magnetotelluric Method*. Cambridge University Press, Cambridge.